Egyptian Geophysical Society
EGS Journal, Vol. 14, No. 1, 123-129 (2016)

MAPPING OF ALTERATION ZONES AT GABAL DARA GRANITES USING ASTER AND AIRBORNE GAMMA RAY SPECTROMETRY DATA

N.M. Abd-El Rahman[(1)], B.M. Ghiath[(2)], Kh. Gemail[(3)] and R.N. Aziz[(2)]

(1) National Authority for Remote Sensing and Space Sciences, Cairo, Egypt.
(2) Nuclear Materials Authority, Cairo, Egypt.
(3) Zagazig University, Sharqiya, Egypt.

رسم نطاقات التغير الحرمائى لجرانيت جبل دارة بإستخدام بيانات الأستر والمسح الجوى لأشعة جاما الطيفية

الخلاصة: كان الهدف الرئيسى من هذا البحث هو تحديد التمعدنات الناتجة عن عمليات التغير الحرمائى فى منطقة جبل دارة والتى تعتبر من أهم المناطق فى الصحراء الشرقية فى مصر من الناحية الإشعاعية. تم معالجة وتحليل بيانات المسح بأشعة جاما الطيفية والاستشعار عن بعد (بيانات الأستر) وذلك لرسم نطاقات التمعدن فى منطقة الدراسة. أظهرت نتائج المسح بأشعة جاما الطيفية أن الجرانيت الحديث فى جبل دارة يعتبر هدفاً هاماً وذلك لاحتوائه على تركيزات عالية من المعادن المشعة كما تم استخدام صور الأستر (L1B) لرسم نطاق التمعدنات المرتبطة بالتغير الحرمائى مثل تجمعات المعادن المرتبطة بالتغير الفيللى والأرجيللى والبروبيلى. تم استخدام طريقة *Feature-oriented Principal Component Selection (FPCS)* فى مجال الطيف المنعكس لرسم التمعدنات المصاحبة لعمليات التغير الحرمائى فى منطقة الدراسة. أظهرت خرائط نطاقات التغير الحرمائى توافقاً جيداً مع مناطق المعادن المستكشفة مما يزيد من احتمالية تواجدها فى المناطق الغير مستكشفة كما يمكن استخدام هذه الخرائط كدليل لعمليات تتبع للمعادن المشعة والاستكشاف المعدنى فى منطقة الدراسة مستقبلا.

ABSTRACT: *The main purpose of this study is to detect the alteration minerals at Gabal Dara area, which is considered one of the most important area sat the eastern desert in Egypt for radioactive exploration. Gamma ray spectrometry and remote sensing ASTER data were processed and analyzed for mapping the mineralization zones in the area. In Gabal Dara area, younger granite was considered as a mapping target due to the high concentration of radioactive materials as indicated from gamma ray spectrometry data. Advanced Space borne Thermal Emission and Reflection Radiometer(ASTER) L1B imagery was used for mapping the alteration mineral zones such as phyllic, argillic and propylitic mineral assemblages. Feature-oriented principal component selection (FPCS) was imposed at ASTER VNIR-SWIR spectral bands with the objective of mapping the occurrence of mineral and members related to hydrothermal alterations* in *Gabal Dara. The constructed alteration maps show good coincidence with the explored mineral resources and suggest further similar unexplored sites. These maps can be used as a guide for further follow-up radioelement and mineral exploration works in the area.*

INTRODUCTION

Large alteration zones, which include Phylic, Argilic and Potassic are usually clear indication of the presence of hydrothermal alteration. Since Hydroxide minerals exist in the areas of Phylic (Sericite and Montmorillonite), Argilic (Alunite and Kaolinite), Propylitic (Chlorite and Calcite), in addition to oxidized minerals especially iron, clay and silicate can also be found in these areas (Boyel, 1979, Bonham, 1989 and Berger and Henley, 1989). These mineral assemblages and others minerals are common in the granitic massive of Gabal Dara area in the Egyptian Eastern Desert which, is considered as one of the most important sites for radioactive exploration. Gabal Dara area is situated, in the North Eastern Desert of Egypt between latitudes 27° 50' N and 28° 05' N and longitudes 32° 50' E and 33° 05' E. It is essentially composed of younger (pink) granites. Gabal Dara possesses an oval shape, which represents an elongated belt of about 28 km in length and an average width of about 25 km, trending N-S direction and occupies approximately 700 km^2 (Fig. 1).

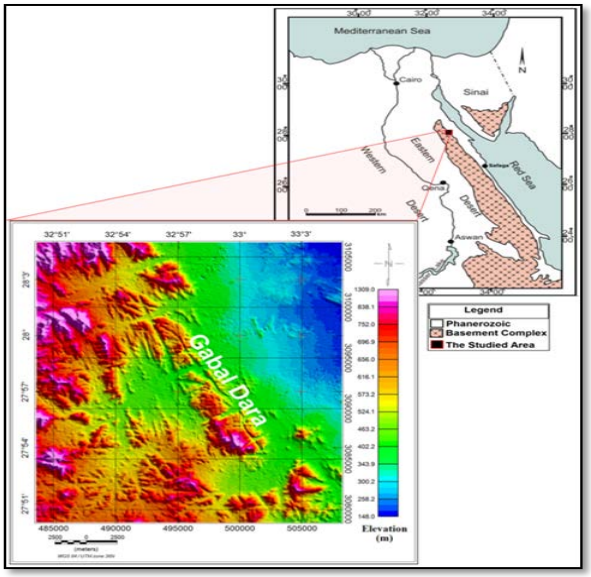

Fig. (1): Base and Shaded color topographic maps of Gabal Dara area, Eastern Desert, Egypt.

Multispectral remote-sensing has been successfully used for lithological and mineralogical mapping especially with the development of the remote sensing sensors and mathematical algorithms that provided detailed information of the mineralogy of the different rock types comprising the Earth's surface (Zhang et al., 2007).

ASTER channels are more continuous in the short wave infrared region than those of Landsat (Zhang et al., 2007), which increase their accuracy in the spectral identification of rocks and minerals (Crosta and Filho, 2003). This has made ASTER data superior to other sensors for lithological mapping (Zhang and Pazner, 2007; Zhang et al., 2007; Gad and Kusky, 2006 and 2007; Raharimahefa and Kusky, 2009).

On the other hand, airborne gamma ray spectrometry can be used as one of the powerful tools in geological mapping, especially in areas of high terrain complex. The conventional approach to the acquisition and processing of airborne gamma ray spectrometric data is to monitor three relatively broad spectral windows. These three elements, potassium (K), equivalent uranium (eU) and equivalent thorium (eTh) windows have energy of 1.46 MeV, 1.76 MeV and 2.62 MeV, respectively (IAEA, 2003). These three elements are used for the measurement of K, U and Th concentrations. Additionally the total count window (TC) gives a measure of the total radioactivity.

ASTER satellite data analysis and airborne gamma ray spectrometric data are fast and economic methods that have been used in geologic mapping and mineral exploration (Crowley et al., 1989; Davis and Guilbert, 1973; Rowan et al., 1996). In the present work, the ASTER and airborne gamma ray spectrometric data were used and integrated for mapping mineralogical patterns and radioactive mineralization zones in the area around Gabal Dara, Eastern Desert. Five minerals were selected to represent the common alteration types in the area. These minerals include chlorite, kaolinite, illite, hematite and seircite.

GEOLOGICALANDMINERALOGICAL SETTING OF GABAL DARA AREA

Gabal Dara area is dominated by presence of both igneous and metamorphic rocks of the basement complex, with the exception of its northeastern corner, which is mainly covered by sedimentary rocks. The exposed rocks belong mostly to the Late Precambrian, early passing to early Paleozoic, except the Phanerozoic Volcanics which belong to Mezosoic age. These rocks are traversed by several wadis filled with Quaternary alluvial deposits (El Shazly, 1977).

The basement complex of the Precambrianage is represented by Metavolcanics, Metagabbro, Older Granitoides, Younger Granites and Phanerozoic cover of Nubian Sandstones and wadisediments.

Figure 2 illustrates the surface geologic map of Gabal Dara area. This map was reconstructed after Conoco Coral and Egyptian General Petroleum Corporation, EGPC (1987) by refreshing colors and clarifying the geologic rock units.

Abd-Elmoneim et al. (1988) studied the geology and radioactivity of G. Dara area. mentioned that G. Dara is essentially composed of younger granites. Structurally, it is highly tectonized, while the prevailing faults and factures are those trending in NNW, NNE and ENE directions. The marginal parts of G. Dara are characterized by the presence of numerous pegmatite bodies in which several radioactive anomalies were recorded. The radiometric and metallographic studies indicate that the high radioactivity mainly of pegmatite bodies is mainly due to the presence of euxenite mineral gains.

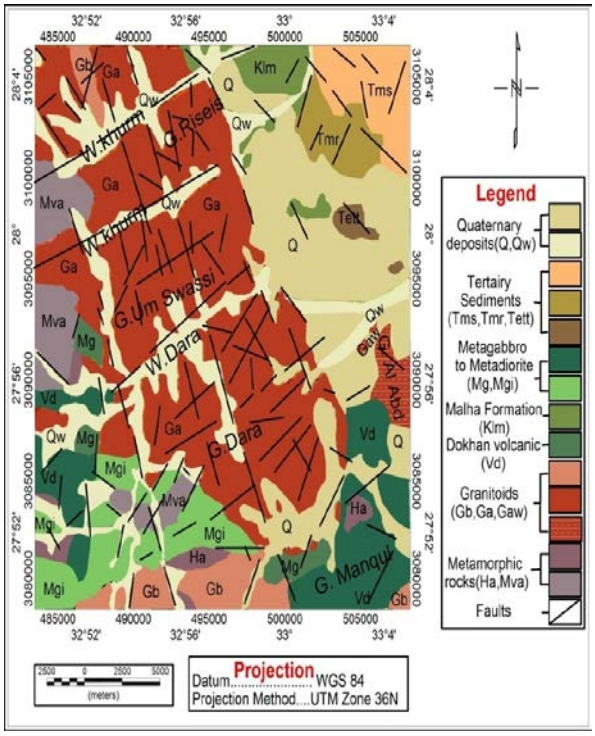

Fig. (2): Compiled geologic map of Gabal Dara area, Eastern Desert, Egypt, (after Conoco & EGPC, 1987).

In Gabal Dara area, the considerable parameters of the mineralized zones of veins and veinlets make it possible to recommend the ore occurrence for more detailed investigations using geophysical and remote sensing data.

METHODS

1. Airborne Gamma ray Spectrometric data:

1.1. Data Acquisition and Processing:

In 1984, cooperation between the Egyptian General Petroleum Corporation, the Egyptian Geological Survey and Mining Authority and Aero-Service Division, Western Geophysical Company of America was formed. Gabal Dara and its surroundings was a part of this survey. The traverse lines took N45° E direction, with a spacing of 1.5 km approximately. The tie lines were perpendicular to the traverse lines (N135° E direction) and spaced about 10 km.

Data processing includes two main categories such as: sources of error and correction of spectral radiometric data. The first one consists of scattering effects, background effect, and atmospheric effects. On the other side the second one, contain background effect, stripping ratio, altitude correction and finally conversion to apparent radiometric concentration.

1.2. Gamma ray Spectrometric Data Analysis:

Airborne spectral radiometric surveying of Gabal Dara area was provided valuable information for four parameters (variables) namely: total count of the gamma radiation (TC in µR/h), absolute concentrations of the three radioelements: potassium (K^{40} in %), equivalent uranium (eU in ppm) and equivalent thorium (eTh in ppm).

Figure 3a shows the spatial distribution of the total radionuclide concentrations of the studied area in younger granites more than other rock types. Separate radio-element maps are also useful to identify certain rock types. For example, the boundaries of the younger granites can be easily delineated from the eU (Fig. 3c) and eTh images (Fig. 3d). The K% maps (Fig. 3b). On the other hand, all spectrometric maps illustrate the boundaries of younger granites and other rock unites in the study area. Gabal Dara area shows higher radioelement values are observed over younger granites. Airborne radioelement concentrations correlate well for the major granitoid plutonic suits.

The three main radiometric element concentrations mainly reflect the lateral variation of surface elemental concentration of different rock and soil types. The major trend that could be traced from the four radiometric maps is the NW trend at Gabal Dara.

The total count map (Fig. 3a) shows three major general levels of radiation, (the lowest level ranges from 2 to 6µR/h) and this range is represented with the pale blue to green color, it is correlated mainly with the Tertiary Sediments. The intermediate level (level 2 from yellow to bright green is ranging from 6 to 9.5 µR/h) and is represented by the green color to yellow. This range is correlated with the Quaternary wadi sediments. The high level (level 3 ranges from 9.5 to 19µR/h) and is represented by the orange, red and magenta colors; this range is correlated mainly with the granitoid rocks (Ga and Gaw in the geological map of figure 2).

Potassium, Uranium and Thorium maps (Figs. 3b, c and d) show the three levels of radiation. The concentration values in level ranges from (0.3, 3.6 %), (1.1, 10.5 ppm eU) and (1.2, 30.9 ppm eTh) for potassium, uranium and thorium maps respectively (all values are multiplied by 10 to show relative variation of the gamma radiation). Also, the highest concentration values of the three parameters are closed to the granitic massive of Gabal Dara.

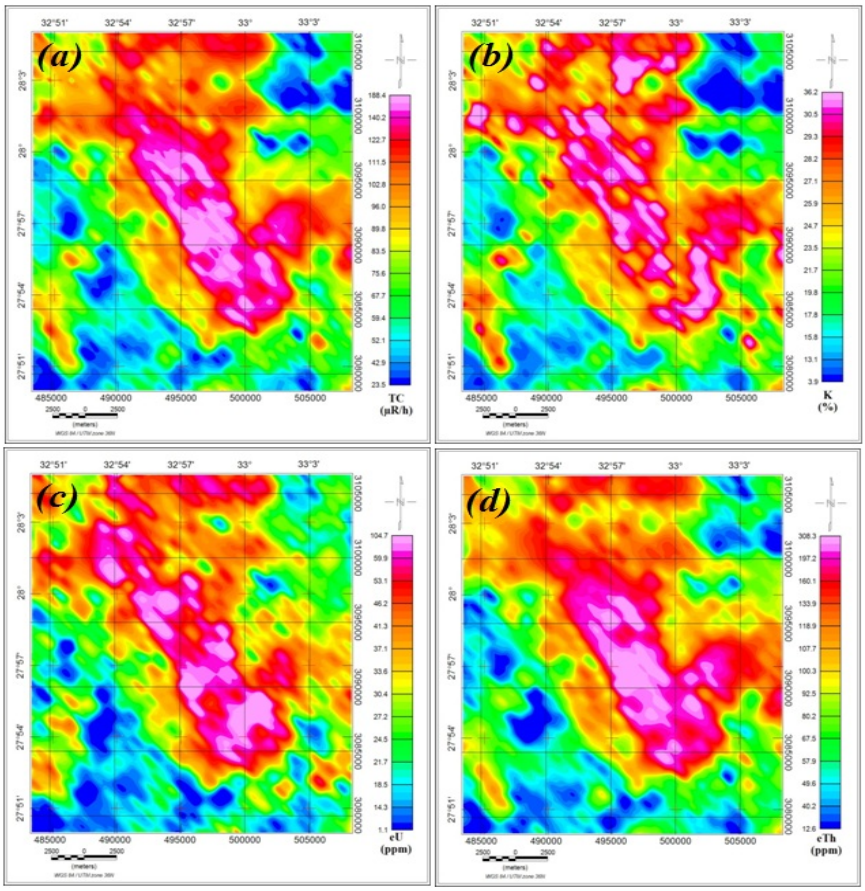

Fig. (3): Spatial distributions and concentrations of radioelements of Gabal Dara area: a) total count (TC), b) potassium (K%), c) equivalent uranium (eU), d) equivalent thorium (eTh). All values are multiplied by 10.

Remote Sensing ASTER data:

ASTER Data and preprocessing:

The ASTER raw data is a raster file composed of a series of layered data points across a grid that spans nearly about 4,500 km^2. So, proper image must be selected with care for attaining the maximum amount of spectral response and accuracy. Two scenes covering the area were used to cover the considered area. These scenes were treated by several levels of pre-processing and enhancement techniques such as Atmospheric Correction (FLAASH), and mosaic king images. Radiometric corrections were applied for ASTER data. Radiometric errors come from the Earth's atmosphere that also needs to be removed for getting a clear image (Scheidt et al, 2008 and Matar and Bamousa, 2013).

ASTER Image Analysis:

Principal component analysis (PCA) is a general method of analysis for correlated multi-variable datasets by mathematical transformation of the original data which are arranged according to the axis of greatest variability for creating new non-correlated components ENVI tutorial.

Principal component is a linear combination of the original spectral bands, so its relationship to the original spectral signatures of targets become not obvious, we used the feature-oriented PC selection (FPCS) method for color composition (Crosta and Moore, 1989).The method comprises examination of the eigenvectors to identify the contributions from original bands (-ve or +ve) to each PC, that help in selecting specific PCs for displaying and concentrating the desired spectral features by highlighting them as bright or dark pixels based on their respective eigenvector values magnitudes and signs (negative eigenvector value indicates absorption while positive ones mean reflectance). This technique was used for mineral exploration on four and six selected bands of Landsat TM data (Crosta and Moore, 1989; Loughlin, 1991; Ruiz-Armenta and Prol-Ledesma, 1998; Tangestani and Moore 2002; Carranza and Hale, 2002) and on ASTER data (Crosta et al, 2003).

Five Alteration end members were selected after field and spectrometric examination, which are: Chlorite, Kaolinite, Illite, Seircite, and Hematite (Table 1).

Table (1): Input bands for FPCS (Crosta) Analysis of the selected minerals.

Minerals	VNIR-SWIR (Reflectance)		Minerals	VNIR-SWIR (Reflectance)	
	High	Low		High	Low
Chlorite	Band 1 Band 5	Band 2 Band 8	Hematite	Band 2 Band 4	Band 3 Band 9
Kaolinite	Band 4 Band 7	Band 6 Band 9	Seircite	Band 4 Band 7	Band 6 Band 8
Illite	Band 4 Band 7	Band 6 Band 8			

Chlorite map:

Mapping chlorite is carried out using ASTER bands 1, 2, 5 and 8 in VNIR-SWIR spectral region. It is remarkable with high reflectance in bands 1 and 5 and low reflectance in bands 2 and 8. Entering these selected bands in a principal component analysis process produced four PCs, the resultant eigenvector values statistics are summarized in Table 2. PC3 shows a high negative loading at band5 (-0.712) and a high positive loading at band8 (0.589), this indicates that chlorite will appear as dark pixels. According to Elsaid et al, (2014) the threshold of chlorite was calculated on PC3 to exclude chlorite lower concentrations by using the equation:

Band DN Threshold = Mean + 2*(Standard deviation)
= 120 + 2*(60) = 240 (1)

Kaolinite:

Kaolinite has a remarkable high reflectance in bands 4 and 7 besides low reflectance in bands 6 and 9 in the VNIR-SWIR spectral region; these four bands were used as input bands in FPCA process producing four PCs with their eigenvector statistics are shown in (Table3).PC2 has high opposite signed loadings for bands 9 (-0.537) and band 4 (0.829), so kaolinite will appear as bright pixels. Thresholding DN value (= 254), (Fig. 5).

Illite:

Illite has high reflectance in bands 4 and 7 besides low reflectance in bands 6 and 8 in the VNIR-SWIR spectral region. Table 4 shows the eigen values result for selected bands. PC4 has high opposite signed loadings for bands 7 (-0.796) and band 8 (0.581), so Illite appears as dark pixels. Thresholding DN value (= 236), (Fig. 6).

Sericite:

As sericite has high reflectance in bands 4 and 7 besides low reflectance in bands 6 and 8 in the VNIR-SWIR spectral region; these four bands are used as input in FPCA process producing four PCs, the eigenvector values statistics are summarized in (Table 5). PC4 has high opposite signed

loadings for bands 7 (-0.796) and band 8 (0.581), so sericite appears as dark pixels. Thresholding DN value (= 238), as shown in (Fig. 7).

Hematite:

The high reflectance of hematite at bands 2 and 4 compared to the low reflectance of bands 3 and 9 used as input bands in FPCA process producing four PCs as in (Table 6). PC4 has a strong negative loading with band 3 (-0.769) and a strong positive loading with band 2 (0.629); this indicates that hematite will appear as dark pixels in PC4 image. (thresholding value = 200) (Fig. 8).

Table (2): Eigenvector values statistics for chlorite.

PC	Band 1↑	Band 2↓	Band 5↑	Band 8↓	Eigen value	Eigen %	Summary statistics of PC3	
PC1	0.504	0.524	0.469	0.502	17077.22	93.24	Min.	0.000
PC2	0.563	0.404	-0.470	-0.547	1105.79	6.04	Max.	255.0
PC3	-0.236	0.301	**-0.712**	**0.589**	95.45	0.52	Mean	120
PC4	0.611	-0.687	-0.230	0.318	37.36	0.20	Std. Dev.	60

Table (3): Eigenvector values statistics for kaolinite.

PC	Band 4↑	Band 6↓	Band 7↑	Band 9↓	Eigen value	Eigen %	Summary statistics of PC2	
PC1	0.469	0.499	0.514	0.516	17019.58	98.19	Min.	0.000
PC2	**0.829**	-0.094	-0.125	**-0.537**	214.84	1.24	Max.	255.0
PC3	0.197	-0.859	0.260	0.394	67.44	0.39	Mean	143.0
PC4	0.234	0.056	-0.808	0.539	31.39	0.18	Std. Dev.	55.5

Table (4): Eigenvector values statistics for Illite

PC	Band 4↑	Band 6↓	Band 7↑	Band 8↓	Eigen Value	Eigen %	Summary statistics of PC4	
PC1	0.468	0.498	0.514	0.519	17097.42	98.33	Min.	0.000
PC2	0.849	-0.099	-0.191	-0.482	197.68	1.14	Max.	255.0
PC3	0.186	-0.859	0.257	0.402	75.18	0.43	Mean	122.4
PC4	0.158	0.068	**-0.796**	**0.581**	16.74	0.10	Std. Dev.	56.8

Table (5): Eigenvector values statistics for Sericite.

PC	Band 4↑	Band 6↓	Band 7↑	Band 8↓	Eigen Value	Eigen %	Summary statistics of PC4	
PC1	0.468	0.498	0.514	0.519	17097.42	98.33	Min.	0.000
PC2	0.849	-0.099	-0.191	-0.482	197.68	1.14	Max.	255.0
PC3	0.186	-0.859	0.257	0.402	75.18	0.43	Mean	124.4
PC4	0.158	0.068	**-0.796**	**0.581**	16.74	0.10	Std. Dev.	56.8

Table (6): Eigenvector values statistics for Hematite.

PC	Band 2↑	Band 3↓	Band 4↑	Band 9↓	Eigen Value	Eigen %	Summary statistics of PC4	
PC1	0.519	0.521	0.462	0.496	17232.71	94.75	Min.	0.000
PC2	0.572	0.358	-0.349	-0.650	740.15	4.07	Max.	255.0
PC3	0.087	0.095	-0.814	0.567	187.68	1.03	Mean	87.4
PC4	**0.629**	**-0.769**	0.049	0.104	27.96	0.15	Std. Dev.	56.3

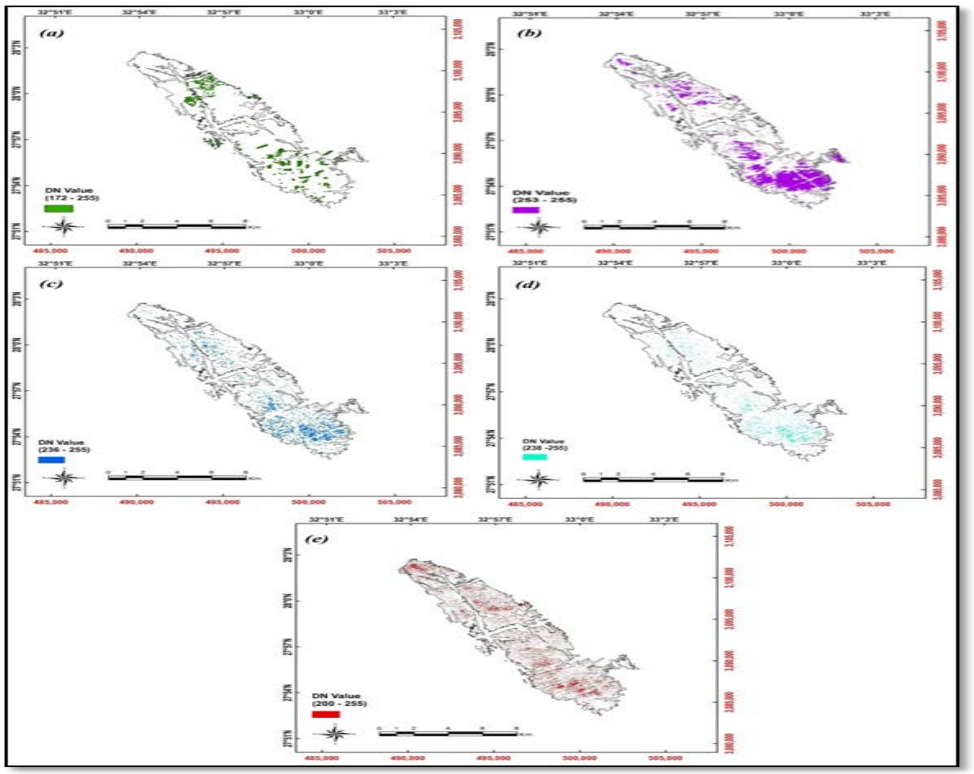

Fig. 4: (a) PC3 Chlorite image using FPCS technique, Green pixels, (b) PC2 kaolinite image using FPCS technique, Magenta pixels, (c) PC4 Illite image using FPCS technique, Blue pixels, (d) PC4 Sericite image using FPCS technique, Cyan pixels, (e) PC4 Hematite image using FPCS technique, Red pixels.

CONCLUSION

By using the Gamma ray Spectrometry data, the higher region of radioactive materials as TC, eU, eTh, and K can be detected in the Younger Granite, which FPCS (crosta) technique carried out on it. The concentration values in highest level ranges from (9.5 to 19µR/h), (2.8, 3.6 %), (4.6, 10.5 ppm eU) and (12.5, 30.9 ppm eTh) for total count, potassium, uranium and thorium maps respectively.

The feature oriented principal component selection (FPCS) technique succeeded in highlighting characteristic spectral features of the common alteration minerals associating radioactive mineralization in Gabal Dara area. PC2 shows the contribution of Kaolinite and PC3 shows the Chlorite mineral and also PC4 shows the contribution of hydroxyl minerals, Sercite and Illite. Crosta technique can be used as a very reliable method for enhancing the areas with alteration minerals as a fast and cheap tool for exploration of radioactive exploration in the Eastern desert.

REFERENCES

Abrams and Hook, 2001. ASTER User Handbook Version 2. Jet Propulsion Laboratory, Pasadena, CA-91109, USA, 135 pp.

Aero-Service Report 1984. Final operational report of airborne magnetic/ radiation survey in the Eastern Desert, Egypt for the Egyptian General Petroleum Corporation. Aero Service, Houston, Texas, April 1984, six volumes.

Berger B.R. and Henley R.W., 1989. Advances in the understanding of epithermal gold–silver deposits, with special reference to the Western United States Economic Geology, 6 (1989), pp. 405–423.

Bonham H.F., 1989. Bulk mineable gold deposits of the Western United States Economic Geology, 6 (1989), pp. 193–207.

Boyel R.W., 1979. The geochemistry of gold and its deposits Geological Survey of Canada, Bulletin (1979), p. 280.

Carranza, E.J.M. and Hale, M., 2002. Mineral imaging with Landsat Thematic Mapper data for hydrothermal alteration mapping in heavily vegetated terrane. International Journal of Remote Sensing 23, 4827 -4852.

Conoco, 1987. Geological Map of Egypt, NF-36 NE Berince, Scale 1: 500,000. Geological survey of Egypt.

Crosta, A. and Moore, J., 1989. Enhancement of Landsat thematic mapper imagery for residual soil mapping in SW Minais Geraisatate, Brazil: a prospecting case history in Greenstone belt terrain,

in: proceedings of the Seventh ERIM Thematic Conference. Remote sensing for Exploration Geology, 1173-1187.

Crosta A.P., Souza Filho C.R., Azevedo F., and Brodie C., 2003. Targeting key alteration minerals in epithermal deposits in Patagonia, Argentina, using ASTER imagery and principal component analysis. Int J Remote Sens; 23: 4233-40.

Elsaid M., Aboelkhair H., Dardier A., Hermas E. and Minoru U., 2014. Processing of Multispectral ASTER Data for Mapping Alteration Minerals Zones: As an Aid for Uranium Exploration in Elmissikat-Eleridiya Granites, Central Eastern Desert, Egypt. The Open Geology Journal, 8, (Suppl 1: M5) 69-83.

ENVI 5.0 Users' Manual, 2012.

Gad, S. and Kusky, T., 2006. Lithological mapping in the Eastern Desert of Egypt, the Barramiya area, using Landsat thematic mapper (TM). Journal of African Earth Sciences, 44(2): 196-202.

Gad, S. and Kusky, T., 2007. ASTER spectral ratioing for lithological mapping in the Arabian–Nubian shield, the Neoproterozoic Wadi Kid area, Sinai, Egypt. Gondwana Research, 11(3): 326-335.

Gupta, R.P., 2003. Remote Sensing Geology, 2nd edition ed. Heidelberg, Springer, Berlin, p. 655.

Jensen, J.R., 2005. Introductory Digital Image Processing. Person Prentice Hall, Upper Saddle River, p. 316.

Matar S.S., and Bamousa A.O. 2013: Integration of the ASTER thermal infra-red bands imageries with geological map of Jabal Al Hasir area, Asir Terrane, the Arabian Shield, Journal of Taibah University for Science 7 (2013) 1–7.

Loughlin W.P., 1991. Principal component analysis for alteration mapping. Photogrammetric Eng Remote Sens; 57: 1163-9.

Perry, J. and Vincent, R., 2009. ASTER brightness and ratio codes for minerals: Application to lithologic mapping in the West Central Powder river Basin, Wyoming. Society of Exploration Geologists. Reviews in Economic Geology 16, 143-168.

Raharimahefa, T. and Kusky, T.M., 2009. Structural and remote sensing analysis of the Betsimisaraka Suture in northeastern Madagascar. Gondwana Research, 15(1): 14-27.

Ruiz-Armenta, J.R. and Prol-Ledesma, R.M., 1998. Techniques for enhancing the spectral response of hydrothermal alteration minerals in Thematic Mapper images of Central Mexico. International Journal of Remote Sensing 19, 1981-2000.

S. Scheidt, M. Ramsey and N. Lancaster, 2008: Radiometric normalization and image mosaic generation of ASTER thermal infrared data: an application to extensive sand sheets and dune fields, Remote Sensing of Environment, 112, 920–933.

Tangestani, M.H. and Moore, F., 2002. Porphyry copper alteration mapping at the Meiduk area, Iran. International Journal of Remote Sensing 23, 4815-4826.

Zhang, X., Pazner, M. and Duke, N., 2007. Lithologic and mineral information extraction for gold exploration using ASTER data in the south Chocolate Mountains (California). Photogrammelry and Remote Sensing, 62: 271-282.